Journal of Experimental Nanoscience
Publication details, including instructions for authors and subscription information:
http://www.informaworld.com/smpp/title~content=t716100757

Detection of negative fullerene conformers

R. F. M. Lobo[a]; B. N. Vicente[a]; F. V. Berardo[a]; I. V. Gouveia[a]; J. H. Ribeiro[a]; P. Pereira[a]
[a] Grupo de Nanotecnologia e Ciência à Nano-Escala (GNCN), Faculdade de Ciências e Tecnologia, Universidade Nova de Lisboa, 2829-516 Caparica, Portugal

To cite this Article Lobo, R. F. M. , Vicente, B. N. , Berardo, F. V. , Gouveia, I. V. , Ribeiro, J. H. and Pereira, P.(2006) 'Detection of negative fullerene conformers', Journal of Experimental Nanoscience, 1: 3, 317 — 332
To link to this Article: DOI: 10.1080/17458080600967247
URL: http://dx.doi.org/10.1080/17458080600967247

Journal of Experimental Nanoscience,
Vol. 1, No. 3, September 2006, 317–332

Taylor & Francis
Taylor & Francis Group

Detection of negative fullerene conformers

R. F. M. LOBO*, B. N. VICENTE, F. V. BERARDO,
I. V. GOUVEIA, J. H. RIBEIRO and P. PEREIRA

Universidade Nova de Lisboa, Grupo de Nanotecnologia e Ciência à Nano-Escala (GNCN),
Faculdade de Ciências e Tecnologia, 2829-516 Caparica, Portugal

(*Received March 2006; in final form July 2006*)

Negative fullerene metastable negative conformers have been detected using electron transfer neutral atom scattering. The anions have been produced through alkali–fullerene collision process, in an energy range well above the ion-pair formation threshold, but still low enough where only the negative parent ion is formed. The interpretation of the parent ion band structure, in time-of-flight spectra, points to the formation of different fullerene conformers, which are favoured by the strong polarization of the cluster anion due to the positive alkali projectile ion. An electric effect operating at nanoscales enables the experimental detection of spheroidal metastable conformers.

Keywords: Fullerenes; Negative conformers; Atom-cluster collisions

1. Introduction

Isomerization in macromolecular systems is important for applications in the fields of nanotechnology and biology. Molecular beams have been used for producing negative species in alkali–fullerene scattering processes, at the post-ion-pair formation energy threshold where only parent fullerene anions are formed [1]. Electron transfer studies in complex molecules have been increasing and here one focuses our particular attention on the fullerenes C_{60} and C_{70}, two of the most significant clusters in nanoscience and nanotechnology. In alkali atom–molecule collisions negative ionization of the molecular target is induced through electron transfer, where the alkali atom donates one electron to the molecule [2–9]. The dynamical study of the ion-pair formation process, $K + C_{60,70} \rightarrow K^+ + C^-_{60,70}$ (M = alkali atom), is probed by using time-of-flight (TOF) mass spectrometry.

Regarding our fullerene targets in this work, advances made in the last decade in the methods to produce C_{60} and C_{70} have resulted in the availability of substantial amounts of these clusters [10, 11].

*Corresponding author. Email: rfl@fct.unl.pt

Journal of Experimental Nanoscience
ISSN 1745–8080 print/ISSN 1745–8099 online © 2006 Taylor & Francis
http://www.tandf.co.uk/journals
DOI: 10.1080/17458080600967247

The sensibility of the technique to the internal nuclear rearrangement of the parent negative ion has been demonstrated for other polyatomic systems [12], where it is possible to estimate the isomerization time in about 1 μs.

The truncated icosahedron shape of buckminsterfullerene is chemically very stable which relies in the Euler pentagon closure principle and pentagon non-adjacency. Randic *et al.*, using electric circuit theory (conjugated-circuit theory of aromaticity) placed these principles on a firm theoretical basis [13]. The several plausible isomers of C_{60} differ in chemical connectivity and most of them will be obviously chemical reactive with dangling carbon bonds and thus less stable.

Theoretical simulations of C_{60} formation have always produced C_{60} with defects [14], and the smallest possible deviation from the perfect buckyball structure is the so-called 'defect' C_{60} [15]. All the atoms in defect C_{60} are still sp^2 bonded. Surprisingly, its binding energy is only 1.6 eV smaller than that of perfect C_{60}. However, the transformation between the perfect and the defect structures is separated by a large energy barrier and thus requires high temperatures and long annealing times [15].

For the neutral cluster C_{60}, most isomers can be constructed by sequential rotations of pairs of carbon atoms about their bond centre, and such a transformation is called 'concerted exchange' or a Stone–Wales transformation, in analogy to a corresponding process in solids [16]. This should be the lowest energy path, since at most two bonds are broken at any point along the path. In order to locate the saddle point along the concerted path trajectory, *ab initio* molecular dynamics adiabatic trajectory simulations have been performed [15]. The transition state (highest point along this path) was found and the saddle point energy is 5.4 eV above that of the defect C_{60}. In experiments, high growth temperatures lead to a much increased yield of C_{60}, but the 5.4 eV barrier is still high enough that even at 1000–2000 K a substantial fraction of C_{60} could be trapped in metastable states. However, no isomers other than buckminsterfullerene have been detected to date. Given the low energy of the defect structure and the height of the barrier, some fraction of defect C_{60} should still survive the formation process (which proceeds in cluster formation via third body collisional cooling to remove the heat generated by the fusion of clusters).

In the neutral C_{60}, there are 1812 possible conformational isomers and 20 of them have more than the 12500 Kekulé which were found for the icosahedral C_{60} [17]. From those 20 isomers most are prolate and a few oblate, three of them being approximately spherical and of those, the isomer with the larger number of Kekulé structures is the prolate with the greatest departure from spherical shape, which means the isomer with the largest structural strain (introduced in curving the planar system of double bonds into a closed cage) [17]. The reason for the additional stability of the neutral icosahedral C_{60} relies in the fact that it is the only one possessing a Kekulé structure where all the hexagons have three double bonds and all the pentagons have only single bonds. The perfect C_{60} indeed has a huge stability which results from the combination of the π electronic stability with a low mechanical structural strain. It is the only isomer possessing isolated pentagons, and their Kekulé structures do not contribute with equal weight for the energy of the electronic ground state [17].

The capture of one electron by the fullerene system results in an electronic configuration which implies a distortion of the carbonaceous cage. In the case of the bucky C_{60}, one can assume that the minimum value for the C_{60}^- radius is similar to the

van der Waals radius of C_{60}, which is about 0.5 nm [18]. Since the calculated HOMO–LUMO gap in neutral defect C_{60} is 0.6 eV smaller than that of neutral buckminsterfullerene [15], one can assume a similar proportion for the HOMO–LUMO gap in both negative ion isomers.

Anion geometry optimization predictions are that upon ion formation, the extra electron should localize mainly in a π^* orbital producing the weakening of the [6:6] bonds [19] and a similar effect has already been confirmed with benzene [20].

The collisional ionization process, $K + C_N \rightarrow K^+ + C_N^-$ ($N = 60, 70$), allows access to metastable states of the negative parent ion which are not attainable in simple electron attachment experiments. Actually, it makes up an efficient way of depositing energy in the form of vibrational excitation of the molecular parent ion [20]. Indeed, working at energies well above the ion-pair formation threshold and below negative fragmentation threshold, it is possible to deposit a significant amount of energy in the target macromolecular ion, given by the endothermicity of the ionization process:

$$\Delta E = I - EA \tag{1}$$

where EA is the fullerene vertical electron affinity and I the potassium atom ionization potential. The fullerene vertical electron maximum corresponds to the largest energy gap between the neutral and the negative fullerene electronic ground states. The amount of energy deposited among the target fullerene ion internal degrees of freedom depends on the endothermicity of the ionization process and not on the collision energy, since the collision time becomes smaller than the intramolecular dynamic characteristic times, which actually happens at energies well above the ion-pair formation threshold [9].

The vibronic excitation is mediated by a crossing of potentials of different electronic states, and the electronic transition transfers the system to another potential hypersurface that is a quite different function of the nuclear coordinates. In order to study the relation between electronic transition and vibrational motion, the most powerful instrumental tool is the molecular beam method [21]. The observation of molecular motion in the subpicosecond domain could be achieved with molecular beam techniques even before the modern femtosecond laser experiments. As the collision energy is in the eV region, one can probe the vibrational dynamics of the parent negative ion on a 10 fs timescale [9].

From the electron harpooning model involving the crossing of ionic and covalent diabatic potential surfaces [2–9], it is roughly possible to infer the K–fullerene critical distance r_c, at which the electronic transition would take place. In fact, since the interaction potential of the neutral system is weak and the ionic attraction potential is due to the sum of the Coulombic attraction term $\sim r^{-1}$ with an induction potential function due to polarization $\sim r^{-4}$, then a lower limit for the crossing distance (in angstroms) can be obtained (if it occurs far enough from the repulsive regions of the two potential surfaces), by the following identity:

$$I - EA = \frac{14.42[1 + \alpha/(2r_c^3)]}{r_c} \tag{2}$$

where I is the well-known ionization potential (in eV) of the electron donor potassium atom (4.33 eV) and α the dc polarizability of the fullerene anion in angstrom^3.

The perfect buckyball has a mean diameter of about 0.70 nm (its cavity almost reaches 0.4 nm in diameter, and the ball's outer diameter is about 1 nm) [22] and its electron affinity EA is about 2.65 eV [23, 24]. The high polarizability and effective number of valence electrons in C_{60} are 86 angstrom^3 and 240, respectively, and C_{60} does not change its polarizability significantly upon ionization [22]. Therefore, the estimated result applying equation (2) is $r_c = 0.9$ nm, which means that the electron transition occurs very close to the buckyball radius in a region where the repulsive forces cannot be neglected, and so these estimations based in a simple potential model, should be taken with severe limitations.

Although very similar in size to C_{60}, the covalent cluster C_{70} shows a lower symmetry and then the degeneracy of electronic states decreases. This fact leads to an increase in the density of electronic states and in the relative number of states with allowed spectroscopic transitions. In addition, C_{70} has a HOMO–LUMO energy gap lower than C_{60} and, thus, it is a better electron donor than the buckyball and a better electron acceptor, as well. The electron affinity of C_{70} is about 2.72 eV [25]. In its turn, its ellipsoidal shape is not far from the ideal spherical, with a mean radius of about 0.75 nm (equatorial diameter of 0.72 nm and distance between polar pentagons 0.79 nm [26]). The C_{70} dc polarizability is even larger than C_{60} and of the order of 97 angstrom^3 [27]. Therefore, applying equation (2) one computes for C_{70} an endoergicity of 1.68 eV (about 0.7 eV smaller than C_{60}) and a critical electron transfer distance of 0.8 nm (i.e. only 0.1 nm shorter than C_{60} but even closer to the neutral C_{70} radius).

Comparison with free electron attachment results are useless in the aim of this work, since this technique is unable to deposit enough energy in the target macromolecular fullerene cluster ion and produce significant vibronic excitation.

2. Experimental

A crossed molecular beam set-up configuration with a neutral fullerene effusive source assembled in the collision chamber, already described elsewhere [1], was used in order to produce a fullerene neutral flux focused in the collision volume. Such a fullerene beam intersects at 90° a fast hyperthermal flux of neutral potassium atoms, formed in a resonant charge exchange source of the Aten type [28]. Such a source has an oven connected with a charge exchange chamber, an ionizer tungsten ribbon and two ion extraction electrodes. K^+ ions are produced by surface ionization of the neutral vapour K atoms, and accelerated with an electric field. By resonant charge exchange, the hyperthermal K^+ ions collide with neutral thermal K atoms, producing fast neutral K atoms. Their energy is given in electron-volts by $0.9\ V_{ion} - 2.4$, where V_{ion} stands for voltage applied to the ionizer. The energy spread of this beam is 0.3 eV and it is collimated by two rectangular slits of 0.2 mm wide. The intensity of the neutral hyperthermal potassium beam is monitored with a surface ionization detector of the Langmuir–Taylor type [21] located in the forward direction prior to the collision volume. The estimated flux in the collision volume is 4.2×10^{12} atoms cm^{-2} s^{-1}.

The fullerene oven is charged with C_{60} powder (99.99% purity from MER Corporation USA) or C_{70} powder (99% purity from Sigma-Aldrich) and by heating it up (typical operation temperatures are in the range of 730 up to 900 K) sublimation

takes place which gives rise to the production of a C_{60} neutral effusive beam. The sublimation temperature of C_{70} at a typical vacuum pressure of 10^{-4} Pa is only about 50 K higher than for C_{60}.

This thermal beam is captured by a cryogenic pump operating at 18 K and located in front of the oven. Through this cryopumping, random molecular reflection by the chamber internal walls is avoided and so noise in the collision volume is reduced.

A schema of the time-of-flight mass spectrometer is shown in figure 1. The negative species formed in the interaction region are extracted normal to the plane of the crossed

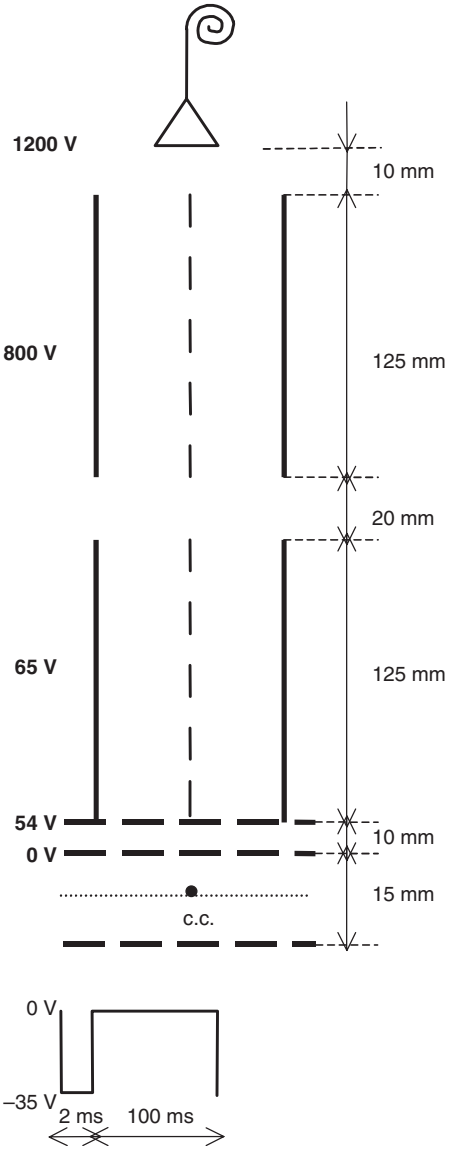

Figure 1. Time-of-flight configuration.

beams by applying a pulsed electric field, 2.0 μs long in a 100 μs duty cycle. Subsequently, they are accelerated into a two drift region time-of-flight mass spectrometer with a total flight path of 27.5 cm. In the first region species were accelerated up to 65 eV and in the second one up to 800 eV. Finally they were accelerated up to 1200 eV and detected with a channeltron electron multiplier.

The interaction volume defined by the intersection of the two beams plays the role of a typical TOF ion source. The actual collision volume geometry is trapezoidal but it can, in a first approximation, be considered a rectangular one, as the difference in the time span will be minimal. Since only single collisions take place in between two pulses, a stationary density of ions n is built up in the source, which is given by the product of the number of anions formed per second and per unit of volume, with the residence time of the ions in the source; this time is equal to the length of the source along the direction of the thermal beam (60 mm) divided by the velocity v of the parent fullerene cluster. When the pulse is started, anions are extracted in the direction perpendicular to the plane of the beams with a velocity much larger than *v*. So the existing ion density is extracted in a time span estimated to be about ten times shorter than the pulse length of 2 μs. This average density, existing during the remainder of the pulse, is very small with respect to the original one. After the 2 μs pulse, a new building up of ion density is started.

The vacuum during the operation of the two beams was kept at 10^{-4} Pa, assuring a single collision performance.

Data acquisition was carried out on a 2046 channel multichannel analyser working in the Pulsed Height Analysis mode. The TOF spectra were obtained after a selected accumulation time considered enough to provide data with good statistics. The multichannel analyser records each TOF spectrum as a function of the channel number *N*. The conversion factor between the multichannel analyser channel number *N* and the time of flight *t* (in microseconds) is dictated by the range of the time analyser (80 μs), being given by:

$$N = 25.6t \tag{3}$$

The intensity for each peak in the spectrum is given by its area which is an invariant quantity with respect to the mass *m* [12]. The full width at half maximum (FWHM) of the parent ion peak displayed in the TOF spectra is proportional to $m^{1/2}$, and the main contribution to the FWHM of the peak comes from the acceleration region [20].

A previous calibration of the TOF spectrometer was done by performing several collisions of neutral potassium atoms with different precursors of the target beam and the result is a best fitted calibration curve for the mass *m* (in daltons, the carbon atomic mass) given by the following expression:

$$m = 4.769 + 0.053N + 4.222 \times 10^{-4}N^2 \tag{4}$$

Collisions of neutral potassium atoms with C_{60} and C_{70} molecules are performed at a few energies above 10 eV, keeping constant the values of the electrostatic potentials in the TOF, accordingly to those displayed in figure 1. Each time-of-flight mass spectrum is recorded at a chosen collision energy within that range.

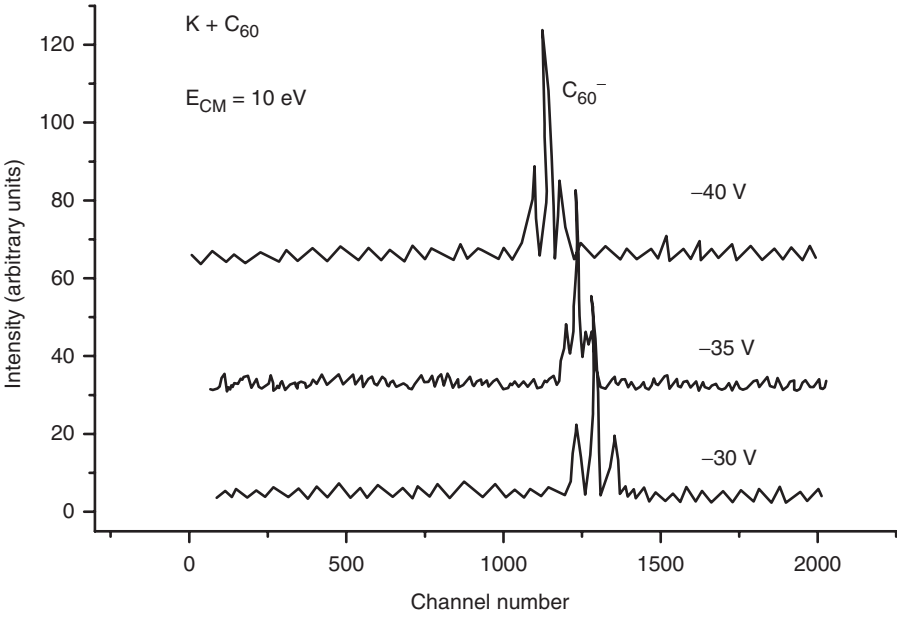

Figure 2. C_{60}^- time-of-flight mass spectra obtained at a center of mass collision energy of 10 eV and C60 oven's temperature of 843 K, for three different pulsed extraction voltages: −30 V, −35 V and −40 V.

3. Results

In the collisions of potassium atoms with C_{60} and C_{70}, performed at low energy (10 eV), the time-of-flight mass spectra show, for −35 V extraction potential, a single well-defined contribution at about $N = 1241$ for C_{60} (figure 2) and $N = 1347$ for C_{70} (figure 3), which according to expressions (3) and (4) can be assigned to the parent fullerene anions C_{60}^- ($60 \times 12 = 720$ dalton) and C_{70}^- ($70 \times 12 = 840$ dalton), respectively.

The reason for not using in addition collision energies below 10 eV lies on the experimental limitation of our charge exchange source, which does not give high enough intensities in order to achieve good signal-to-noise ratios in the accumulation TOF spectra.

All the spectral intensities are normalized to the primary alkali beam intensity which is monitored with the Langmuir–Taylor detector, and so they are displayed in inverse units of electric current per second.

For $K + C_{60}$ and $K + C_{70}$ collisions the TOF spectra recorded at a fixed collision energy (10 eV) and different pulsed voltages (−30 V, −35 V and −40 V) show evidence of the formation of a most intense parent negative ion accompanied on both sides by satellite peaks (figures 2 and 3). The choice for the close proximity in those pulsed extraction voltage values was made in order to avoid the need for correcting the other voltages on the TOF grids due to ion refocusing reasons.

Figure 4 displays the TOF spectra obtained for $K + C_{60}$ at two higher collision energies, just to illustrate that fragmentation patterns are already present.

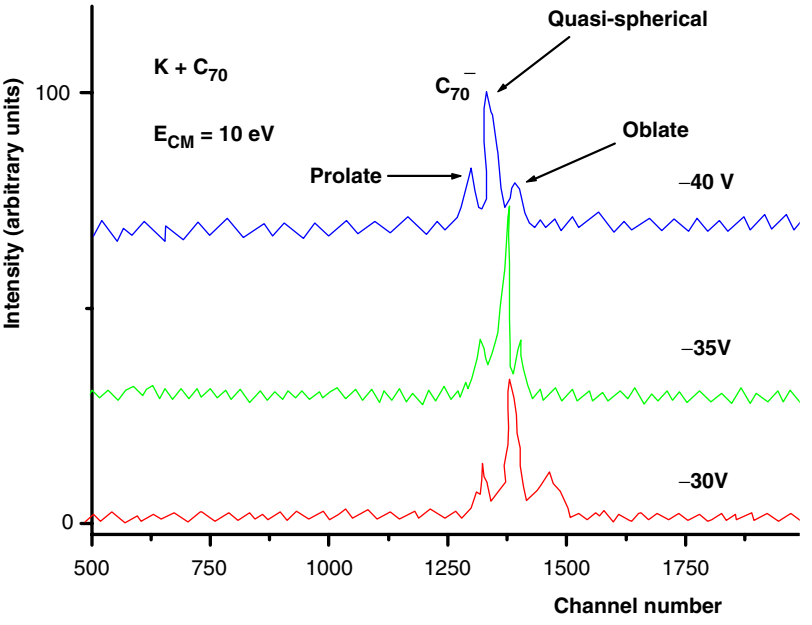

Figure 3. C_{70}^- time-of-flight mass spectra obtained at a center of mass collision energy of 10 eV and C70 oven's temperature of 900 K, for three different pulsed extraction voltages: −30 V, −35 V and −40 V.

The density of the target molecular beam in the collision region is not monitored, although the intensity of the target beam is assumed to not vary significantly (as the oven temperature is kept constant, for each target fullerene used).

4. Discussion

C_{60} and C_{70} parent ions reveal themselves as very stable anions in the experimental collision energy range.

In a simple quantum-chemical description of the electronic structure of C_{60} based on the molecular orbital (MO) approach, each carbon atom contributes with four valence orbitals (2s, $2p_x$, $2p_y$ and $2p_z$) and thus C_{60} has 120 occupied molecular orbitals and 120 unoccupied or virtual MO's. With some approximations (C_{60} is not planar) 60 MO's (30 occupied and 30 virtual) can be considered of π type and the remaining 180 orbitals of σ type. In analogy with large aromatic compounds, the highest occupied MOs (HOMOs) and the lowest unoccupied MOs (LUMOs), which determine the lower electronically excited states are of σ type. The electronic ground state of C_{60} is a closed shell. The lowest electronic absorption of C_{60}^- is theoretically expected to occur at about 0.6 eV, where the electron in the T_{1u} ground state orbital makes a transition to the T_{1g} orbital [29].

The amount of energy deposited among the internal degrees of freedom of the target fullerene ion depends (at collision energies well above the ion-pair formation threshold) on the endothermicity of the ionization process and becomes independent of the

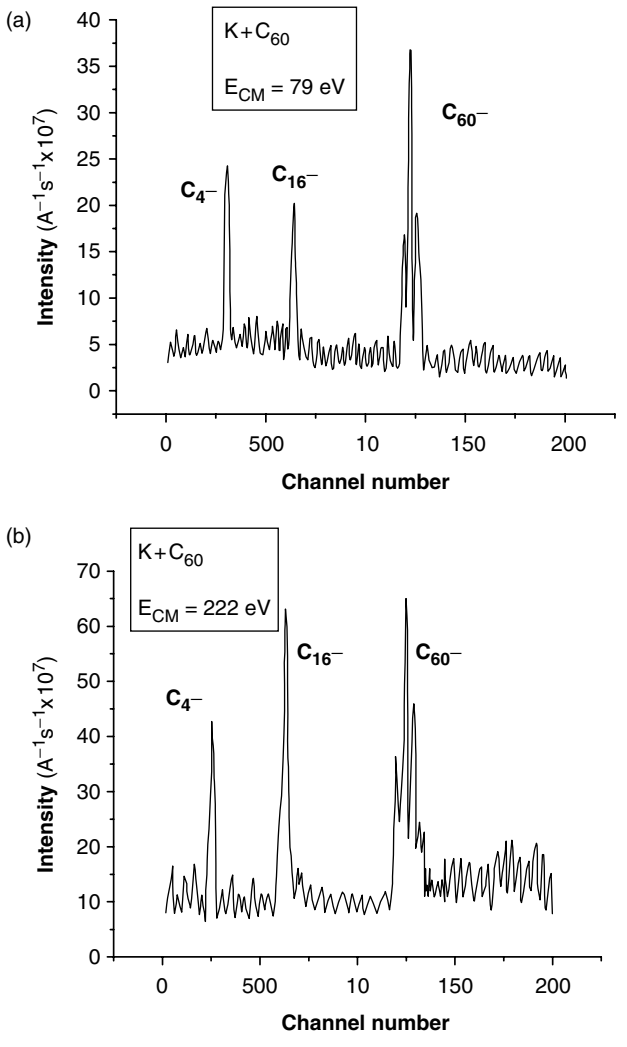

Figure 4. C_{60}^- TOF spectra recorded at two high collision energies and pulsed extraction voltage of −35 V. C60 oven's temperature is 843 K.

collision energy, as long as the collision time is smaller than the intramolecular characteristic times. This is the reason why at high collision energies the satellite peaks are still present (see figure 4).

Two satellite contributions have been observed in the band structure of C_{60}^- and C_{70}^- parent-ion TOF spectra (located on both sides of the main central peak), as it is clearly displayed in figures 2 and 3. This effect in the spectra was only observed for the parent ion contribution and it is not present for the ionic fragments. The time shift corresponding to the observed satellite peaks in the C_{60}^- and C_{70}^- TOF spectra are, respectively, of the order of 1–3 and 2–4 μs, relatively to the central main peak.

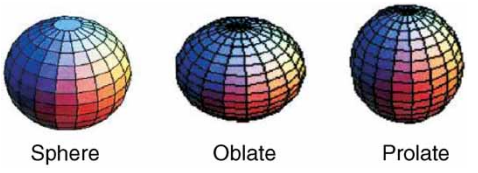

Figure 5. Negative fullerene spheroidal shapes.

According to the common available tables of isotopic masses and natural abundances, the carbon isotopes ^{12}C and ^{13}C represent, respectively, about 98.9% and 1.1% of the total number of natural carbon atoms in C_{60}. Therefore this distribution of isotopic masses is completely unable to explain the two observed satellite peaks in the TOF spectra. Moreover, the corresponding mass shifts with respect to the central C_{60}^- peak, observed in the TOF spectra, are much smaller than 12 dalton (the carbon atomic mass), and then one cannot explain the two small peaks by eventual abstraction or addition of a carbon atom to the negative buckyball cage.

These facts seem to point to the formation of distinct conformational metastable C_{60}^- and C_{70}^- isomers (prolate and oblate), which can be formed in the diabatic negative potential surface. Since the calculated HOMO–LUMO gap in neutral defect C_{60} is 0.6 eV smaller than that of neutral buckminsterfullerene [15], one can assume a similar proportion for the HOMO–LUMO gap in both negative ion isomers.

This presumed detection of different spheroidal metastable C_{60}^- conformers (figure 5) was made possible due to an electric effect operating at the nanoscale. Actually, for a negative spheroidal conductor (note that the additional electron in the cage is completely delocalized) immersed in a uniform extraction electric field, its need to keep a zero electric field inside imposes an asymmetric surface charge distribution, which in the neighbourhood of the fullerene cage distorts the applied surrounding uniform electric field, and gives rise to an electric field gradient along the linear dimension of the anion macromolecular cage, in the direction of the applied field (see figure 6). Actually, this field gradient is not negligible compared with the fullerene diameter. Since the field gradient is dependent on the shape assumed by the fullerene cage, the extraction force applied to the negative ion will be different for each possible negative conformer (prolate, oblate and sphere).

Detection of the fullerene metastable negative conformers has been achieved using electron transfer atom scattering, which allows the depositing of a significant amount of internal energy in the fullerene anions. This was not made possible by other closely related techniques, as for instance in the case of near-grazing surface scattering of neutral C_{60} with surface targets [33], where the energies involved are lower by several orders of magnitude. In addition, performing Penning ionization collisions of thermal C_{60} with supersonic metastable rare-gas atoms Rg, it is possible to detect C_{60}^+ ions and electrons, and explain the results assuming an intermediate ionic state Rg^+–C_{60}^- [34], which influences the energy distribution measurements of the ejected electrons. However, with this technique the collision energies are very small and then it was not possible to gain indirect information on metastable negative states of C_{60}.

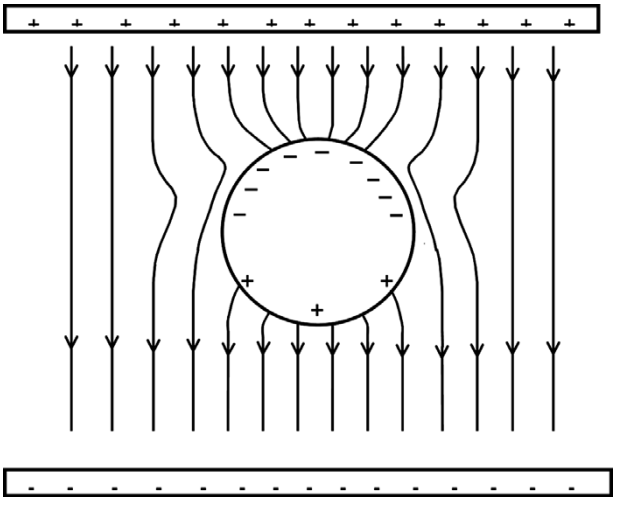

Figure 6. Negative charged sphere in an applied uniform electric field.

Table 1. Estimated and experimental C_{60}^- time-of-flight differences with respect to the spheroidal conformer at different extraction voltages. Since the prolate conformer appears at the lowest time-of-flights, their time shifts are reported as negative in opposition with the oblate delays which are considered positive.

	−30 V			−35 V			−40 V		
C_{60}	TOF (μs)	Δt_{teo} (μs)	Δt_{exp} (μs)	TOF (μs)	Δt_{teo} (μs)	Δt_{exp} (μs)	TOF (μs)	Δt_{teo} (μs)	Δt_{exp} (μs)
oblate	50.0	+3.7	+2.6	46.3	+3.4	+2.5	43.4	+3.2	+2.2
prolate	43.5	–2.8	–1.6	40.3	–2.6	–1.5	37.8	–2.4	–1.3
sphere	46.3	–	–	42.9	–	–	40.2	–	–

Table 2. Estimated and experimental C_{70}^- time-of-flight differences with respect to the spheroidal conformer at different extraction voltages. Since the prolate conformer appears at the lowest time-of-flights, their time shifts are reported as negative in opposition with the oblate delays which are considered positive.

	−30 V			−35 V			−40 V		
C_{70}	TOF (μs)	Δt_{teo} (μs)	Δt_{exp} (μs)	TOF (μs)	Δt_{teo} (μs)	Δt_{exp} (μs)	TOF (μs)	Δt_{teo} (μs)	Δt_{exp} (μs)
oblate	57.0	+4.4	+3.5	52.8	+4.1	+3.1	49.5	+3.9	+2.8
prolate	49.2	–3.4	–2.3	45.6	–3.1	–2.0	42.7	–2.9	–1.9
sphere	52.6	–	–	48.7	–	–	45.6	–	–

Tables 1 and 2 summarizes the ion times of flight obtained with our estimations, for each conformational isomer at the three experimental extraction potentials.

The formation of such conformational isomers is likely to be induced by the strong polarization of the fullerene anion in the presence of the K^+ projectile ion, during the collision lifetime.

When the positive charge of the K^+ ion is closely interacting with the highly polarizable fullerene anion, an electric dipole is induced, and this polarization effect

is likely to induce the stabilization of some anion spheroidal conformers. These metastable negative states together with the ground negative state (sphere) should be adiabatically coupled at large distances.

The three observed conformational isomers should correspond to the most stable states resulting from the multiple carbon atoms interactions. The spherical conformer has a zero quadrupole electric moment and is the most stable. When we are considering the oblate and prolate conformations, we are most likely assuming an average among all the possible isomers (which in the neutral C_{60} are known to be 20, as explained in the introduction of this work).

In our calculations, for both C_{60} and C_{70} clusters, the oblate shape takes more time than the spherical perfect isomer to travel through the flight path, and in turn the prolate shape will be the first of the three to be detected. Therefore, according to our model, the satellite contribution appearing at the largest time of flight in the spectra should correspond to the oblate isomer and the satellite peak appearing earlier can be assigned to the corresponding prolate isomers.

Also according to the calculations (see tables 1 and 2), the stronger the applied extraction field, the earlier the prolate reaches the detector and in turn the oblate isomer will arrive with an even larger delay. This is in clear agreement with the experimental variation of the satellite time shifts with the extraction field magnitude. Actually, as can be confirmed from figures 2 and 3, the stronger the applied electric field, the larger are such time shifts. Moreover, the estimated time shift variations agree, in a first approximation, with the experimental ones.

At low collision energies the relative areas of the two satellite contributions in the TOF spectra are quite similar, and as long as more energy is put into the collision, the contribution at the higher time of flight seems to become more relevant. This could indicate that as more internal energy is deposited in the parent ion by the collision, the more likely it is that the formation of the oblate isomer contribution, and so, in the negative ion, the oblate metastable state should correspond to a higher energy than the prolate state. Note that (see the introduction of this paper) in the neutral C_{60} cluster there are more prolate shaped isomers than oblate isomers.

The fact that the two satellite peaks for the parent ion contribution are present in the TOF spectra even at a large collision energy is a clear indication that their relevance does not significantly depend on the collision time.

The explanation for the longer time shifts observed for C_{70}^- isomers in comparison with those of C_{60}^- (about 0.6 μs) probably does not rely on the slight difference between their respective neutral endoergicity values involved in the electron transfer scattering process (otherwise, the lower endoergicity of C_{70} should not result in a larger internal energy deposited in the parent ion) but on the stronger polarizability effect of the K^+ ion in the case of the C_{70} electron cloud during the collision time. This time is, for identical collision energies, mainly determined by the critical electron transfer distance, which is quite similar for both carbon clusters.

5. Fullerene anion conformers flight times

The calculated difference in time of flight between the fullerene anion spherical mass and each of the other two spheroidal isomers is of the same order of magnitude as that

experimentally observed in the case of C_{60} (1–3 μss) and C_{70}, as well. The calculations are inspired in simple classical electrodynamic estimations of the fullerene anion time of flight (based on the TOF mass spectrometer electric potentials and lengths displayed in figure 1) and in the surface charge density σ of a conducting ellipsoid [30]. Such calculations have been performed making use of the *Mathematica 5.1* program [31, 32], for a spheroidal eccentricity of 0.9 (i.e. semimajor axis length double the semiminor axis) which corresponds to a deformation parameter of 1.5.

5.1. *Surface charge density for a conducting spheroidal body*

An ellipsoidal surface can be expressed in Cartesian coordinates by [31, 32]:

$$\frac{x^2}{a^2}+\frac{y^2}{b^2}+\frac{z^2}{c^2}=1 \tag{5}$$

and the surface charge density σ on a conducting ellipsoid can be written [30]:

$$\sigma=\frac{q}{4\pi abc\sqrt{(x^2/a^4)+(y^2/b^4)+(z^2/c^4)}} \tag{6}$$

which in the case of a spheroidal surface takes the simplified form [30]:

$$\sigma=\frac{q}{4\pi abc\sqrt{((x^2+y^2)/a^4)+(z^2/c^4)}} \tag{7}$$

where a, b and c are the lengths of the three ellipsoid axis (with $a=b$) and q is the total charge, which in the case of the fullerene negative ion will assume the electron charge value: $q=-e=-1.6\times10^{-19}$ coulomb. In the case of an oblate shape we have $a>c$ and in the prolate shape, $a<c$.

5.2. *Calculation of a spheroidal elementary surface*

In the case of a spheroidal surface of revolution (oblate or prolate), obtained by the rotation of a line $r=r(z)$ around the z axis, the expression for r is the following [31, 32]:

$$r(z)=a\sqrt{1-\left(\frac{z}{c}\right)^2} \tag{8}$$

and the corresponding elementary surface dS is given by [31, 32]:

$$dS=2\pi r\sqrt{1+\left(\frac{dr}{dz}\right)^2}dz \tag{9}$$

From (8) and (9) it is then possible to find the expression for the spheroidal elementary surface:

$$\mathrm{d}S = 2\pi a\sqrt{1+\frac{(a-c)(a+c)z^2}{c^4}}\,\mathrm{d}z \tag{10}$$

5.3. *Electrostatic force applied on the fullerene anion*

By replacing dS and the surface charge density σ in the expression of the elementary force:

$$\mathrm{d}F = \mathrm{d}qE = \mathrm{d}SE \tag{11}$$

(where E represents the total electrostatic field) one can obtain three expressions for the three components of the force relative to each of the spatial coordinates:

$$\mathrm{d}F_x = \frac{q^2x}{4\pi a^3c^4\varepsilon_0}\left(\frac{c^2-z^2}{a^2c^2}+\frac{z^2}{c^4}\right)^{(-3/2)}\sqrt{1+\frac{(a-c)(a+c)z^2}{c^4}} \tag{12}$$

$$\mathrm{d}F_y = \frac{q^2y}{4\pi a^3c^4\varepsilon_0}\left(\frac{c^2-z^2}{a^2c^2}+\frac{z^2}{c^4}\right)^{(-3/2)}\sqrt{1+\frac{(a-c)(a+c)z^2}{c^4}} \tag{13}$$

$$\mathrm{d}F_z = \sqrt{1+\frac{(a-c)(a+c)z^2}{c^4}}\left[\frac{q^2z}{4\pi a^3c^4\varepsilon_0}\left(\frac{c^2-z^2}{a^2c^2}+\frac{z^2}{c^4}\right)^{(-3/2)}+\frac{qE_{ap}}{2ac}\left(\frac{c^2-z^2}{a^2c^2}+\frac{z^2}{c^4}\right)^{(-1/2)}\right] \tag{14}$$

where E_{ap} is the applied uniform electric field (given experimentally by the ratio between the extraction pulse voltage and the distance between the parallel extraction electrodes), which is equal to $(E-\sigma/\varepsilon_0)$, with ε_0 being the vacuum electric permittivity.

In our simulations we have ignored the components of the force relative to the x and y coordinates, because they would not produce any effect on the time of flight of the ion.

In a first approximation, if one considers that negative electric charge is only distributed on the upper half of the spheroidal isomer, the component z of the force will be computed by the integral of dF_z, for z between $-c$ and c. The z component of the force will then assume a different value for each of the three isomers.

5.4. *Simulation of the time of flight*

Taking into account the geometrical configuration of the TOF mass spectrometer (figure 1), the total time of flight t for the anion is estimated by application of classical equations of motion, applied to each of the six identified path lengths (in figure 1),

considering the two drift and the four acceleration regions, where t_j and t_i stand for the corresponding times:

$$t = \sum_{i=1}^{4} t_i + \sum_{j=1}^{2} t_j \quad \text{with } t_i = m\frac{v_0^i + \sqrt{-v_0^{i2} + (2F_i/m)(x_i - x_{0i})}}{F_i} \quad \text{and} \quad t_j = \frac{x_j - x_{0j}}{v_0^j} \tag{15}$$

where m is the ion mass, F_i is the computed electric force in each acceleration region of the spectrometer, $v_0^{j,j}$ are the initial velocities in each step region of the mass spectrometer and $(x_{i,j} - x_{0i,j})$ are their respective lengths.

Acknowledgements

This work has been developed with support from FCT/MCTES, in particular through the project POCTI/FIS/43627/2000.

References

[1] R.F.M. Lobo, N.T. Silva. Neutral C60 effusive source for atom–molecule electron transfer collisions. *Rev. Scient. Instrum.*, **72**, 3505 (2001).
[2] D.R. Herschbach. Reactive scattering in molecular beams. *Adv. Chem. Phys.*, **10**, 319 (1966).
[3] A. Baede, J. Los. Total cross sections for charge transfer and production of free electrons by collisions between alkali atoms and some molecules. *Physica*, **52**, 422 (1971).
[4] S. Wexler, E.K. Parks. Molecular beam studies of collisional ionization and ion-pair formation. *Annu. Rev. Phys. Chem.*, **30**, 179 (1979).
[5] E.W. Rothe, S.Y. Tang, G.P. Reck. Anion production from $Cs + CF_3X$: evidence for stripping. *Chem. Phys. Lett.*, **26**, 434 (1974).
[6] R.N. Compton, P.W. Reinhardt, L.D. Cooper. Collisional ionization between alkali atoms and some methane derivatives: electron affinities for CH_3NO_2, CF_3I, and CF_3Br. *J. Chem. Phys.*, **68**, 4360 (1978).
[7] P.R. Brooks. Reactions of oriented molecules. *Science*, **193**, 11 (1976).
[8] K. Lacmann. Collisional ionization. *Adv. Chem. Phys.*, **42**, 513 (1980).
[9] A.W. Klein, J. Los, E.A. Gislason. Vibronic coupling at intersections of covalent and ionic states. *Phys. Rep.*, **90**, 1 (1982).
[10] H.W. Kroto, J. Heath, S. O'Brian, R.F. Curl, R.E. Smalley. C_{60}-buckminsterfullerene. *Nature*, **318**, 162 (1985).
[11] W. Krätchmer, L.D. Lamb, K. Fostiropoulos, D.R. Huffman. Solid C_{60}: a new form of carbon. *Nature*, **347**, 354 (1990).
[12] R.F.M. Lobo, A.M.C. Moutinho, K. Lacmann, J. Los. Excitation of the nitro group in nitromethane by electron transfer. *J. Chem. Phys.*, **95**, 4360 (1991).
[13] M. Randic. Conjugated circuits and resonance energies of benzenoid hydrocarbons. *Chem. Phys. Lett.*, **38**, 68 (1976).
[14] J. Chelikowsky. Nucleation of C_{60} clusters. *Phys. Rev. Lett.*, **67**, 2970 (1991).
[15] J. Yi, J. Bernholc. Isomerization of C_{60} fullerenes. *J. Chem. Phys.*, **96**, 8634 (1992).
[16] K.C. Pandey. Diffusion without vacancies or interstitials: A new concerted exchange mechanism. *Phys. Rev. Lett.*, **57**, 2287 (1986).
[17] S.J. Austin, P.W. Fowler, P. Hansen, D.E. Manolopoulos, M. Zheng. Fullerene isomers of C60: Kekule counts versus stability. *Chem. Phys.Lett.*, **228**, 478 (1994).
[18] J. Huang, H.S. Carman, R.N. Compton. Low-energy electron attachment to C_{60}. *J. Phys. Chem.*, **99**, 1719 (1995).

[19] R.F.M. Lobo, N.T. Silva, and M.S. Costa, Negative fragmentation and internal nuclear rearrangement of C_{60}^- in electron transfer atom–molecule collisions. In *Proceedings XXI International Symposium on Molecular Beams*, IESL, Ed. FORTH, University of Crete, Hersonisos, GR (2005).
[20] R.F.M. Lobo, P.L. Vieira, S.S.M.C. Godinho, M.J. Calhorda. Mono-halobenzenes anion fragmentation induced by atom–molecule electron-transfer collisions. *J. Chem. Phys*., **116**, 9712 (2002).
[21] G. Scoles. *Atomic and Molecular Beam Methods*, Oxford University Press, New York (1988/1992) Vol. 1 and 2.
[22] W.E. Billups, M.A. Ciufolini. *Buckminsterfullerenes*, VCH Publishers, New York (1993).
[23] H. Lorents, M. Mathur. Fullerene–fullerene collisions: Fragmentation and electron capture. *Phys. Rev. A*, **52**, 3847 (1995).
[24] H. Yasumatsu, T. Kondow, H. Kitagawa, K. Tabayashi, K. Shobatake. Absorption spectrum of C_{60} in the gas phase: Autoionization via core-excited Rydberg states. *J. Chem. Phys*., **104**, 899 (1996).
[25] O. Boltalina, L. Siderov, A.Y. Borschevskii, E.V. Sukhanova, E.V. Skokan. Electron affinities of higher fullerenes. *Rap. Commun. Mass Spectrom*., **7**, 1009 (1993).
[26] K. Hedberg, C.A. Brown, R.D. Johnson. Molecular structure of free molecules of the fullerene C_{70} from gas-phase electron diffraction. *J. Am. Chem. Soc*., **119**, 5314 (1997).
[27] M.S. Dresselhaus, G. Dresselhaus, P.C. Eklund. *Science of Fullerenes and Carbon Nanotubes*, Academic Press, San Diego (1998).
[28] J.A. Aten, J. Los. Space charge related energy deficit in beams from charge exchange Sources. *J. Phys. E. Sci. Inst*., **8**, 408 (1975).
[29] B. Friedman. Electronic absorption spectra in C_{60}^- and C_{60}^+. *Phys. Rev. B*, **48**, 2743 (1993).
[30] L.D. Landau, E.M. Lifshitz. *Electrodynamics of Continuous Media*, Pergamon Press, New York (1960).
[31] R.J. Gaylord, S. Kamin, P. Wellin. *Introduction to Programming with Mathematica*, Springer-Verlag, New York (1993).
[32] M.L. Abell, J.P. Braselton. *Differential Equations with Mathematica*, 2nd ed., Academic Press, Boston (1996).
[33] A. Bekkerman, B. Tsipinyuk, S. Verkhoturov, E. Kolodney. Negative ion formation in near grazing surface scattering of hyperthermal C_{60}: Image charge effects. *J. Chem. Phys*., **109**, 8652 (1998).
[34] B. Brunetti, P. Candori, R. Ferramosche, S. Falcinelli, F. Vecchiocattivi, A. Sassara, M. Chergui. Penning ionization of C_{60} molecules. *Chem. Phys. Lett*., **294**, 584 (1998).